DOI: 10.2352/ISSN.2470-1173.2016.12.IMSE-048

# A Time-of-Flight CMOS Range Image Sensor Using 4-Tap Output Pixels with Lateral-Electric-Field Control

*Taichi KASUGAI† Sang-Man HAN† Hanh TRANG† Taishi TAKASAWA† Satoshi AOYAMA‡*
*Keita YASUTOMI† Keiichiro KAGAWA† and Shoji KAWAHITO†*
*†Research Institute of Electronics, Shizuoka University, 3-5-1 Johoku, Naka-ku, Hamamatsu, Shizuoka, 432-8011, Japan*
*‡Brookman Technology, Daihatsujisho Bldg. 10F, 125 Daikumachi, Naka-ku, Hamamatsu, Shizuoka, 430-0936, Japan*
*E-mail: tkasu@idl.rie.shizuoka.ac.jp TEL: +81-53-478-1342 FAX: +81-53-412-5481*

## Abstract

*This paper presents a 160×240-pixel CMOS Time-of-Flight (TOF) range imager with a 4-tap charge modulator using pinned-photodiode high-speed lock-in pixels in a 0.11µm CIS process. The proposed lock-in pixel structure using lateral electric field (LEF) control is suitable for implementing a multiple-tap charge modulator while achieving high-speed charge transfer for high time resolution. A CMOS TOF range imager with the multiple-tap charge modulators is expected to have background light cancelling capability in one frame and to improve range resolution with shifted short double light pulses. In this paper, we report the design, implementation and evaluation results of the TOF range imager using the 4-tap LEF modulator (LEFM). The TOF range imager has a range resolution of less than 3.2mm for the range from 1.0m to 2.0m at the frame rate of 15.7fps.*

## Introduction

Time-of-Flight (TOF) range imagers have a wide range of application such as gesture-based remote controllers, amusements, robot eyes, security systems, car-mounted camera, virtual reality and so on. The TOF range imaging is a rapidly developing technique for video rate 3D imaging. Recently, various developments of TOF range imagers have been reported [1-6]. The reported CMOS TOF range imagers often use single-tap or two-tap lock-in pixels, which require two or four frames to make range imaging. These architectures have a weak point for the range measurement of moving objects under background light. If pixels have three or more output ports, it makes possible to measure the range image of moving objects under background light with less motion artifacts. In general, there is a trade-off between maximum measurement range and range resolution in the TOF range imaging. For improving range resolution, we may use a shorter light pulse. However, the maximum measurement range is reduced by shortening the light pulse.

To address these problems, this paper presents a CMOS TOF range imager with 4-tap lateral electric field charge modulator (LEFM) pixels using pinned photodiode-based technology [7, 8]. The proposed lock-in pixel structure using lateral electric field (LEF) control is suitable for implementing a multiple-tap charge modulator while achieving high-speed charge transfer and high demodulation contrast for high time resolution. A CMOS TOF range imager with the multiple-tap charge modulators is expected to have background light cancelling capability in one frame and to improve the range resolution with shifted short double light pulses without reducing measurement range.

The rest of this paper is organized as follows: the operation principle of the pixel and the TOF range imager design, the experimental results of the implemented chip, conclusions, and acknowledgements.

## Pixel and TOF range imager design

### Lock-in pixel with LEFM

Fig. 1 shows the structure of 2-tap photo-charge modulator. In this modulator called the lateral electric field charge modulator (LEFM), 3 sets of gates (G1, G2 and GD) for applying lateral electric field (LEF) are used for charge transportation in the depleted pinned photodiodes. The gates are not used for transferring charge through the gate, but used for controlling electric field perpendicular to the gate. To do this, a positive voltage (e.g., High = 2.0V) and negative voltage (e.g., Low = -1.0V) are used for the operation. The direction of photoelectron flow in a pinned photodiode is controlled by the gates, and time-resolved signal detection and accumulation are carried out in the two floating diffusions (FD1 and FD2). For example, when the G1 is High, the potential of the LEFM (see profiles of X-X' in Fig. 1) attracts photo electrons generated in the aperture region to be transferred to FD1. The gate GD is used for periodical charge draining for small duty-cycle operation for TOF measurements. During signal readout, GD is also High and other gates are Low for preventing the influence of background light (see profiles of X-X' and Y-Y' in Fig. 1). The doping concentration of the p-type epitaxial layer and surface $p^+$ layer for hole pinning are optimized for realizing large potential modulation in the pinned-photodiode.

By using this technique, we have implemented a 4-Tap LEFM with a drain for TOF range imager. Fig. 2 shows the structure of LEFM with 4-tap outputs and a drain. Each modulator has 4 outputs (FD1, FD2, FD3 and FD4) and 4 drains to which the charge transfer is controlled by 5 sets of gates (G1, G2, G3, G4 and GD). Using the LEFM with 4-tap output, the range can be estimated with background light cancelling, and the range resolution is improved with shifted short double light pulses without reducing the measurement range.

### Operation principles

The timing diagram for range shift operation with a small duty-ratio double light pulse is shown in Fig. 3. The gate pulse width of G1, G2, G3 and G4 is given by $R_D T_C$, where $T_C$ is the cycle time and $R_D$ is duty ratio of the gate pulse to the cycle time. Then, the gate pulse width of GD is given by $(1\text{-}4R_D)T_C$. The signal light pulse width and the time of flight of the received light are denoted by $T_0$ and $T_d$, respectively. The signals from FD1, FD2, FD3 and FD4 are denoted by S1, S2 S3 and S4, respectively. In TOF method, the equation for estimating the range is given by

$$L = \frac{1}{2}cT_d \quad (1)$$

where L is the range, c is the speed of light.

In the case of received light (2) in Fig. 4, the difference of the amount of charges between the two FDs (FD1, FD2) reflects the

©2016 Society for Imaging Science and Technology
DOI: 10.2352/ISSN.2470-1173.2016.12.IMSE-048

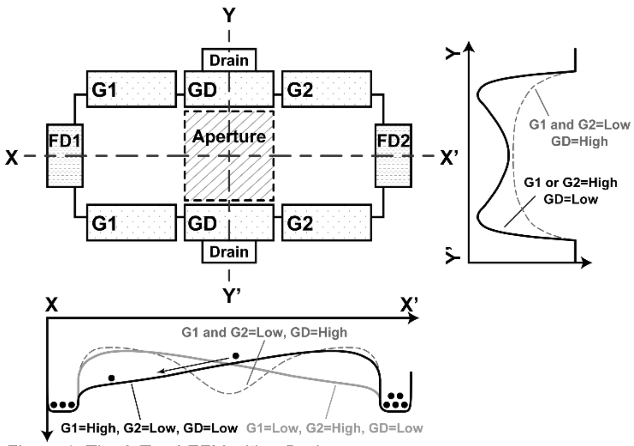


*Figure 1: The 2-Tap LEFM with a Drain*

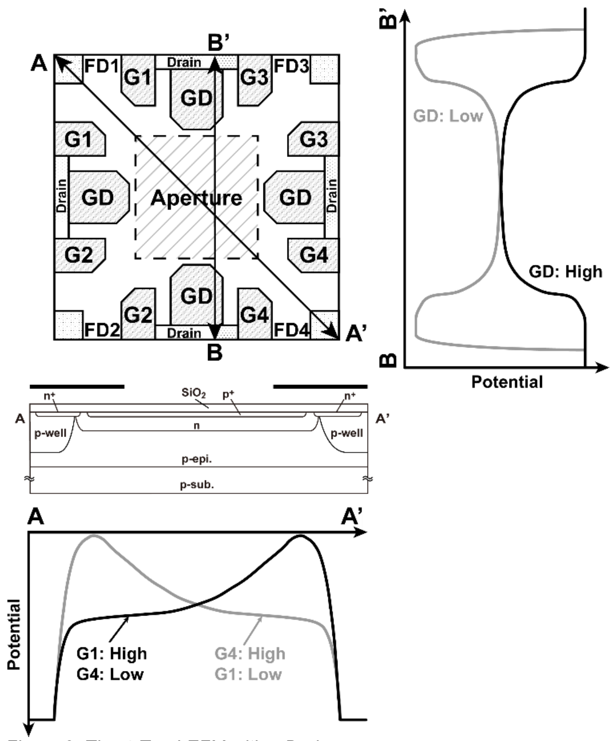


*Figure 2: The 4-Tap LEFM with a Drain*

time-of-flight of light pulse $T_d$. The range is calculated by the TOF-dependent charges. During G1 is activated and the other gates are deactivated, a part of the signal light pulse is received, and the signal charge $Q_1$ is stored in FD1. The $Q_1$ is expressed as

$$Q_1 = I_S(T_0 - T_d) \tag{2}$$

where $I_S$ is the photo current generated by the signal light pulse. In the next phase where G2 gates are activated and the other gates are deactivated, the rest part of the light pulse is received and the signal charge $Q_2$ stored in FD2 is expressed as

$$Q_2 = I_S T_d \tag{3}$$

If the background light exists, Eq. 2 and Eq. 3 are modified as

$$Q_1 = I_S(T_0 - T_d) + I_{BL} R_D T_C \tag{4}$$

$$Q_2 = I_S T_d + I_{BL} R_D T_C \tag{5}$$

where $I_{BL}$ is photo current generated by the background light and $R_D T_C$ is the gate pulse width.

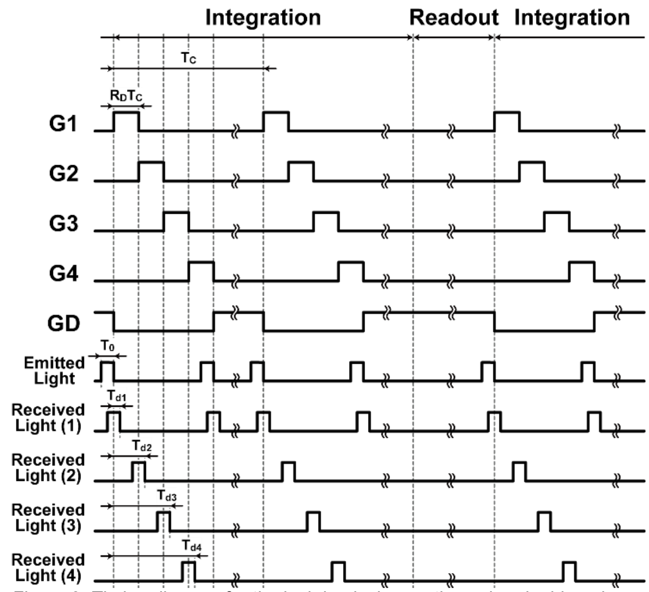


*Figure 3: Timing diagram for the lock-in pixel operation using double pulses*

| | |
|---|---|
| $0 < \mathrm{TOF} < R_D T_C$ | $\mathrm{TOF} = T_0 \frac{Q_1 - Q_3}{Q_1 + Q_4 - 2Q_3}$ |
| $R_D T_C < \mathrm{TOF} < 2R_D T_C$ | $\mathrm{TOF} = R_D T_C + T_0 \frac{Q_2 - Q_4}{Q_2 + Q_1 - 2Q_4}$ |
| $2R_D T_C < \mathrm{TOF} < 3R_D T_C$ | $\mathrm{TOF} = 2R_D T_C + T_0 \frac{Q_3 - Q_1}{Q_3 + Q_2 - 2Q_1}$ |
| $3R_D T_C < \mathrm{TOF} < 4R_D T_C$ | $\mathrm{TOF} = 3R_D T_C + T_0 \frac{Q_4 - Q_2}{Q_4 + Q_3 - 2Q_2}$ |

*Figure 4: Range shift operation for extending the measurement range using shifted short double light pulses*

In order to cancel the background light, FD3 and FD4 are used for taking background light charges only. The electrons generated by background light are transferred from pinned photo diode to the FDs. The signal charges $Q_3$ and $Q_4$ stored in FD3 and FD4 are expressed as

$$Q_3 = Q_4 = I_{BL} R_D T_C \tag{6}$$

The background light cancelling is done by the subtraction of back-ground-only signals from the signals with received signal lights. In this case, $Q_1$ and $Q_2$ are TOF-dependent signals and $Q_3$ and $Q_4$ are background-only signals. The equation for estimating the range in each pixel is given by

$$L = \frac{1}{2} c T_d = \frac{1}{2} c T_0 \cdot \frac{Q_2 - Q_4}{Q_1 + Q_2 - 2Q_4} \tag{7}$$

In the rest of time in one cycle, photoelectrons generated in the photodiode due to background light or slow carrier components generated by the signal light pulse are drained. To do this, GD gates are activated and the other gates are deactivated.

In TOF range imagers using periodical pulsed light, there is a trade-off between maximum measurement range and range resolution. For improving range resolution, we may just use short light pulse. However, on the other hand, the measurement range is reduced by shortening light pulses. By switching TOF-dependent signals and background-only signals for TOF measurement depending on the zone of TOF as shown in Fig. 4, the range resolution is improved while attaining wide measurement range.

©2016 Society for Imaging Science and Technology
DOI: 10.2352/ISSN.2470-1173.2016.12.IMSE-048

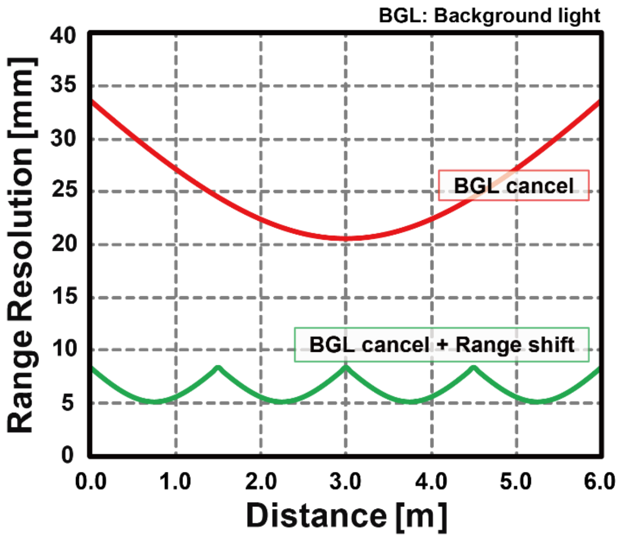


*Figure 5: Calculated range resolution*

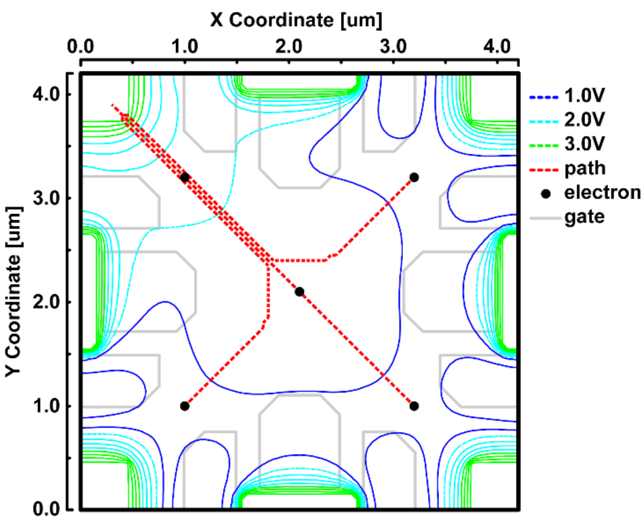


*Figure 6: Charge transfer simulation results*

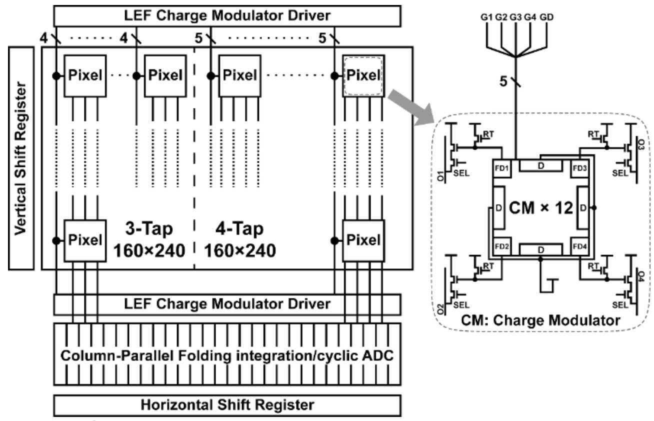


*Figure 7: Sensor architecture*

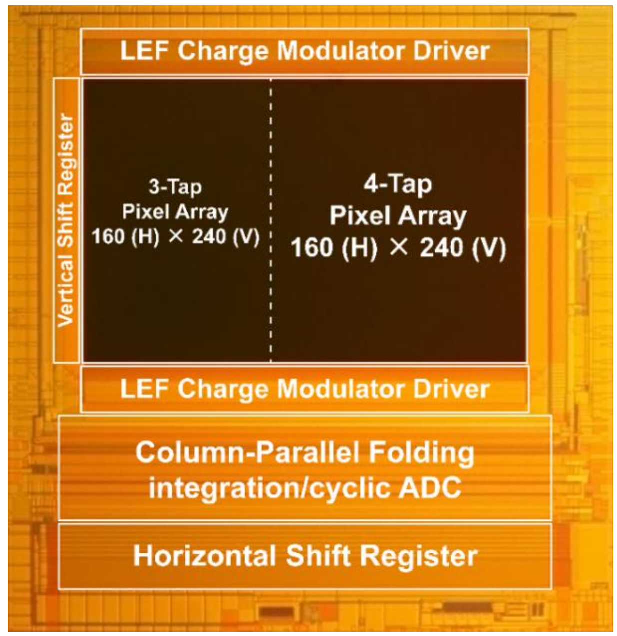


*Figure 8: Chip micrograph*

For example, if the light pulse is coming as shown in "Received light (3)" in Fig. 3, the delay time $T_{d3}$ is easily obtained by the $Q_1$, $Q_2$, $Q_3$, and $R_D T_C$, but a range-shifting of $2R_D T_C$ must be considered. The range is simply calculated by this equation similar to the received light (1). The range resolution is improved by using shifted short double light pulse without reducing the measurement range. Fig. 5 shows calculated range resolution. The equation to calculate the range resolution is given by [9]

$$\sigma_L = \frac{cT_0}{2C_{DC}\sqrt{N_S}}\sqrt{R_S(1-R_S)+2(R_B+R_R)(1-3R_S+3{R_S}^2)} \quad (8)$$

where $C_{DC}$ is the demodulation contrast, $R_S = N_{TOF}/N_S$, $R_B = N_B/N_S$, and $R_R = N_R^2/N_S$. The number of total signal electrons is denoted by $N_S$ which is the sum of signal electrons stored in FD1 and FD2. The signal electrons stored in FD2 is proportional to the $T_d$, and it is denoted by $N_{TOF}$. The number of electrons due to background light stored in FDs is denoted by $N_B$. The readout noise expressed as the number of electrons is denoted by $N_R$. In the theoretical calculation, $N_S$ of 100,000, $N_B$ of 81,000, $N_R$ of 140, and $C_{DC}$ of 0.80 are used. Background light cancelling capability and the use of shifted short double light pulses achieve a wide measurement range which is four times of the conventional method. In other words, this method achieves higher range resolution which is approximately four times of that without shortening the measurement range.

A TOF range imager using the 4-tap lock-in pixels is designed and implemented using 110nm 1P4M CIS technology with lightly-doped relatively thick epi-layer on a p-type substrate. Fig. 6 shows plots of equipotential lines and trace of carrier transportations when High is applied to G1 and Low is applied to the others. The black dots indicate the initial position of electrons before moving by the electric fields, the red dashed lines indicate the trace of movement of electrons and the gray lines indicate the 5 sets of gates. The direction of the electron flow is controlled by the gate voltages.

### *The sensor architecture*

The block diagram of the TOF range imager is shown in Fig. 7. The TOF range imager consists of a 160×240 pixel array, vertical and horizontal shift register, ADC, and LEF charge modulator driver. Each pixel has four SF outputs which are shared by twelve charge modulators. Each of the four outputs from each pixel are connected each of the column ADC and are converted to digital codes in parallel using high-resolution folding integration/cyclic ADCs [10].

DOI: 10.2352/ISSN.2470-1173.2016.12.IMSE-048

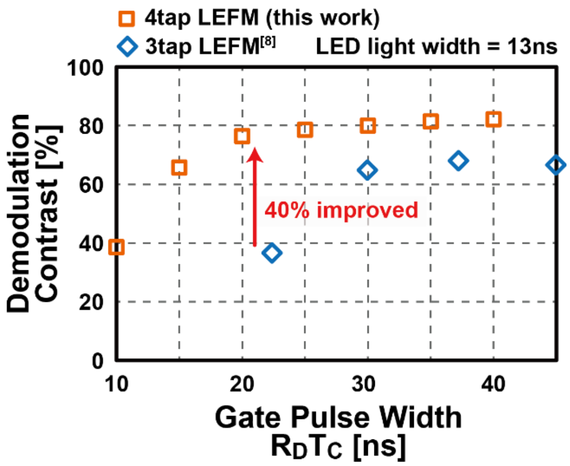


Figure 9: Demodulation contrast

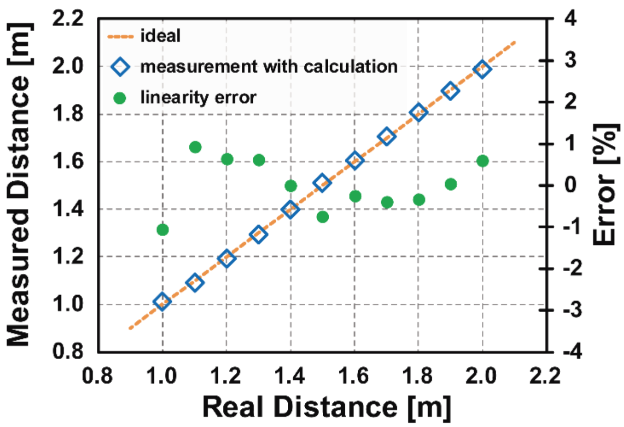


Figure 10: Measured linearity and nonlinearity

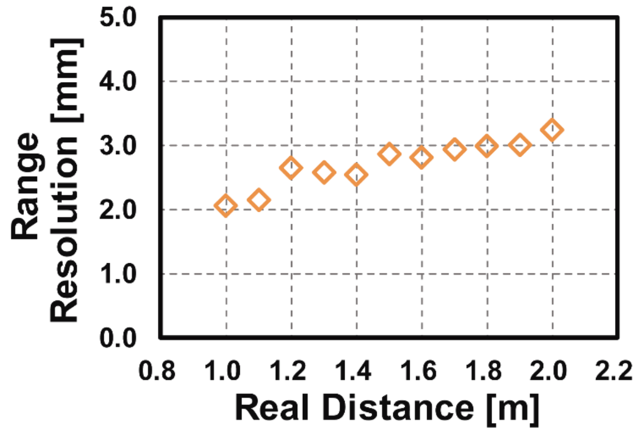


Figure 11: Measured range resolution versus real distance

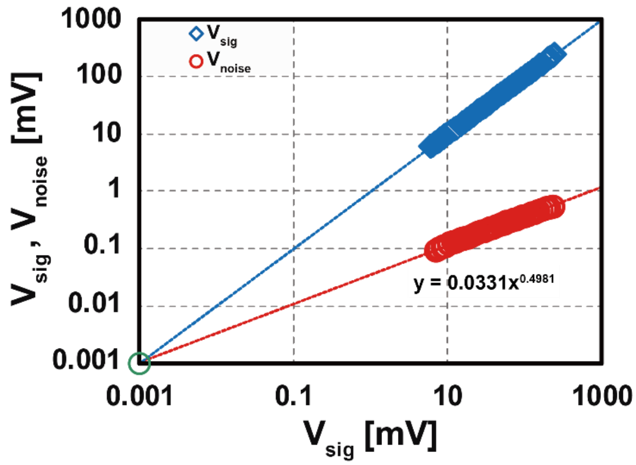


Figure 12: Photon transfer curve

## Experimental Results

The chip micrograph is shown Fig.8. The size of the whole chip is 9.0mm × 9.3mm. The signal light source is composed of 96 near-infrared LEDs with the 870nm wavelength, and the signal light pulse width $T_0$ is set to 13ns. The cycle time of exposure $T_C$ and the duty ratio $R_D$ are 1.0μs and 0.02, respectively. The gate pulse width $R_DT_C$ for G1, G2, G3 and G4 is 20ns. For seamless range shift measurement, the light pulse width must be equal to or wider than that of the gating pulses. In this measurement, $T_0$ of 13ns for the purpose of demonstration of high range resolution due to high-speed response of the pixel. The frame rate is 15.7fps. A lens with a focal length of 12.5mm and an F-number of 2.0 are mounted on the sensor. An infrared bandpass filter is placed in front of the lens. The High level for gate voltage of G1, G2, G3 and G4 is set to 2.5V, and the Low level is set to -1.0V. The High level for gate voltage of GD is set to 3.6V, and the Low level is set to -1.0V.

### *Demodulation Contrast*

Fig. 9 shows a measured demodulation contrast under the various gate pulse width $R_DT_C$. These measurement results are obtained by the average of 10 frames in 10×10 pixels in the center of the array. A white flat panel is located at 1.0m. The high de-modulation contrast of 80% is obtained for the gate pulse width of larger than 30ns. The degradation when the gate pulse width is reduced is mainly due to the degradation of switching speed of the gate-driver for the modulators.

The demodulation contrast is defined as [3, 11]

$$C_{DC} = \frac{|S_1 - S_2|_{MAX}}{(S_1 + S_2)} \qquad (9)$$

where $S_1$ and $S_2$ are the signals from FD1 and FD2, respectively. $|S_1 - S_2|_{MAX}$ is the peak to peak signal of the measured value, and $(S_1 + S_2)$ is proportional to the offset.

### *Linearity and Range resolution*

Fig. 10 shows a measured linearity and nonlinearity error, and Fig.11 shows a measured range resolution as a function of distance. These measurement results are obtained by the average of 30 frames of raw data in 10×10 pixels in the center of the array with a white flat panel. A panel is located between 1.0m and 2.0m with the step of 0.1m. The gate pulse width is 20ns.

In Fig. 9, the slop and offset are calibrated at the distance of 1.0m and 2.0m. To compensate the sensitivity and time offset due to the demodulation contrast and the delay of electronic circuits, Eq. 7 for estimating the range is modified as

$$L = \frac{1}{2}c\left(T_0 \cdot \frac{Q_2 - Q_4}{Q_1 + Q_2 - 2Q_4} \cdot \frac{1}{C_{DC}} - T_{OS}\right) \qquad (10)$$

where $T_{OS}$ is the time offset. The slop is calibrated by the demodulation contrast, and, the offset is calibrated by the time offset. The nonlinearity error which is the maximum difference of the measured range from real range is 1.1%.

DOI: 10.2352/ISSN.2470-1173.2016.12.IMSE-048

In Fig. 11, the range resolution is the standard deviation of the temporal deviation of measured range. The high range resolution of 2.1mm to 3.2mm is achieved when background light is turned off.

Fig. 12 shows photon transfer curve. The conversion gain is 1.1μV/e$^-$.

## Conclusion

This paper presented a CMOS TOF range imager with 4-tap LEFM using pinned-photodiode high-speed lock-in pixels. A CMOS TOF range imager with multiple-tap charge modulators provides background light cancelling capability in one frame and improves the range resolution with shifted double light pluses method. The high demodulation contrast of 80% is achieved by the developed TOF range imager. The high range resolution of 2.1mm to 3.2mm is obtained for the range from 1.0m to 2.0m in this measurement. By using range shifting technique, the high resolution can be obtained in 4-times longer range that is 1m to 5m, for instance. Table 1 summarizes the specification and characteristics of this work. The performance of the TOF imager developed in this work is compared with the TOF range imagers recently reported as shown in Table 2.

## Acknowledgements

This work was partly supported by the JSPS Grant-in-Aid for Scientific Research (S), No. 25220905 and JST COI STREAM.

**Table 1: Sensor specification**

| | |
|---|---|
| Process | 0.11 μm 1P4M CIS |
| Total area | 9.0 mm (H) x 9.3 mm (V) |
| Power supplies | 1.5 V (Digital),<br>3.3 V (Analog, Digital) |
| Emitter | 96 LED array<br>with 870 nm wavelength |
| Lens | F# 2.0 / focal length of 12.5mm |
| Number of pixels | 160 (H) x 240 (V) (4-Tap pixels) |
| Pixel size | 22.4 μm (H) x 16.8 μm (V) |
| Conversion Gain | 1.1 μV/e$^-$ |
| Fill factor | 41 % (with micro lens) |
| Frame rate | 15.7 fps (exposure time of 50ms) |
| Modulation speed | 13 ns (Light width)<br>20 ns (Gate width) |
| Demodulation Contrast | 76.9 % @20ns (Gate width) |
| Measured range | 1.0 ~ 2.0 m |
| Non linearity | 1.1 % |
| Range resolution | 2.1 ~ 3.2 mm |

## References

[1] R. Lange, P. Seitz, A. Biber and S. Lauxtermann, “Demodulation Pixels in CCD and CMOS technologies for Time-of-Flight Ranging,” Proc. SPIE, vol.3965, pp. 177-188, 2000.

[2] S. Kawahito, I. A. Halin, T. Ushinaga, T. Sawada, M. Homma, and Y. Maeda, “A CMOS time-of-flight range image sensor with gates-on-field-oxide structure,” IEEE Sensors J., vol. 7, no.12, pp. 1578-1586, Dec. 2007.

[3] D. Stoppa, N. Massari, L. Pancheri, M. Malfatti, M. Perenzoni, and L. Gonzo, “A Range Image Sensor Based on 10um Lock-In Pixels in 0.18um CMOS Imaging Technology,” IEEE J. Solid-State Circuits, vol. 46, no.1, pp. 248-258, Jan. 2011.

[4] S. J. Kim, B. Kang, K. D. K. Kim, K. Lee, C. Y. Kim, and K. Kim, “A 1920x1080 3.65μm-pixel 2D/3D image sensor with split and binning pixel structure in 0.11 μm standard CMOS,” ISSCC Dig. Tech. Papers, pp. 396-397, Feb. 2012.

[5] O. Shcherbakova, L. Pancheri, G.-F. Dalla Betta, N. Massari, and D. Stoppa, “3D camera based on linear-mode gain-modulated avalanche photodiodes,” ISSCC Dig. Tech. Papers, pp. 490- 491, Feb. 2013.

[6] A. Payne, A. Daniel, A. Mehta, B. Thompson, C. S. Bamji, D. Snow, H. Oshima, L. Prather, M. Fenton, L. Kordus, P. O’Connor, R. McCauley, S. Nayak, S. Acharya, S. Mehta, T. Elkhatib, T. Meyer, T. O’Dwyer, T. Perry, V.-H. Chan, V. Wong, V. Mogallapu, W. Qian, and Z. Xu, “A 512×424 CMOS 3D Time-of-Flight image sensor with multi-frequency photo-demodulation up to 130MHz and 2GS/s ADC,” ISSCC Dig. Tech. Papers, pp. 134-135, Feb. 2014.

[7] S. Kawahito, G. Beak, Z. Li, S.-M. Han, M.-W. Seo, K. Yasutomi, and K. Kagawa, “CMOS Lock-in Pixel Image Sensors with Lateral Eelectric Field Cotrol for Time-Resolved Imaging,” Proc. 2013 Int. Image Sensor Workshop (IISW), pp. 361-364, Jun. 2013.

[8] S.-M. Han, T. Takasawa, T. Akahori, K. Yasutomi, K. Kagawa, and S. Kawahito, “A 413×240-pixel sub-centimeter resolution Time-of-Flight CMOS image sensor with in-pixel background canceling using lateral-electric-field charge modulators,” ISSCC Dig. Tech. Papers, pp. 130-131, Feb. 2014.

[9] S.-M. Han, T. Takasawa, K. Yasutomi, A. Satoshi, K. Kagawa, and S. Kawahito, “A Time-of-Flight Range Image Sensor with Background Cancelling Lock-in Pixels Based on Lateral Electric Field Charge Modulation,” IEEE J. Electron Devices Society, vol. 3, no. 3, pp. 267-275, May. 2015.

[10] M.-W. Seo, S.-H. Suh, T. Iida, T. Takasawa, K. Isobe, T. Watanabe, S. Itoh, K. Yasutomi, and S. Kawahito, “A Low-Noise High Intrascene Dynamic Range CMOS Image Sensor With a 13 to 19b Variable-Resolution Column-Parallel Folding-Integration/Cyclic ADC,” IEEE J. Solid-State Circuits, vol.47, no.1, pp. 272-283, Jan. 2012.

[11] E. Tadmor, A. Lahav, G.Yahav, A. Fish and D. Cohen, “A Fast-Gated CMOS Image Sensor with a Vertical Overflow Drain Shutter Mechanism,” IEEE Trans. Electron Devices, vol. 63, pp. 138-144, Jun. 2015.

DOI: 10.2352/ISSN.2470-1173.2016.12.IMSE-048

**Table 2: Performance comparison**

| | This work | S.-M. Han, et al. [8] | O. Shcherbakova, et al. [5] | S. J. Kim, et al.[4] |
|---|---|---|---|---|
| Number of pixels | 160 x 240 (4-Tap pixels) | 320 x 240 | 64 x 64 | 480 x 270 |
| Pixel size [$\mu m^2$] | 22.4 X 16.8 | 16.8 x 16.8 | 30 x 30 | 14.6 x 14.6 |
| Fill factor [%] | 41 (with microlens) | 55 (with microlens) | 25.75 | 38.5 |
| Lens F# | 2.0 | 2.0 | 1.2 | 1.6 |
| Illumination wavelength [nm] | 870 | 870 | 850 | 850 |
| Illumination power [mW] | 250 | 250 | 21 $W/m^2$ (peak power @ 1m) | 700 |
| Frame rate [fps] | 15.7 | 15 | 50 / 200 | 11 |
| Modulation speed | 13 ns (Light width) 20 ns (Gate width) | 13 ns (Light width) 30 ns (Gate width) | 25 MHz | 20 MHz |
| Measured range [m] | 1.0 ~ 2.0 | 0.8 ~ 1.8 | 2 ~ 4.75 @50fps | 0.75 ~ 4.5 |
| Non linearity [%] | 1.1 | 1.03 | 1.7 | 0.93 |
| Range resolution [mm] | 2.1 ~ 3.2 | 4.0 ~ 6.4 | 19 ~ 57 @50fps | 10 ~ 38 |
| In-pixel Background light Cancelling | Yes | Yes | No | No |
| Frames to make Range image | 1 frame | 1 frame | 4 frame | 2 frame |